Preheating after $\mathcal{N}$-flation

Diana Battefeld* and Shinsuke Kawai+

Helsinki Institute of Physics, P.O. Box 64, University of Helsinki, FIN-00014 Helsinki, Finland

(Received 14 March 2008; published 9 June 2008)

We study preheating in $\mathcal{N}$-flation, assuming the Marčenko-Pastur mass distribution, equal-energy initial conditions at the beginning of inflation and equal axion-matter couplings, where matter is taken to be a single, massless bosonic field. By numerical analysis we find that preheating via parametric resonance is suppressed, indicating that the old theory of perturbative preheating is applicable. While the tensor-to-scalar ratio, the non-Gaussianity parameters and the scalar spectral index computed for $\mathcal{N}$-flation are similar to those in single-field inflation (at least within an observationally viable parameter region), our results suggest that the physics of preheating can differ significantly from the single-field case.

DOI: 10.1103/PhysRevD.77.123507 PACS numbers: 98.80.Cq

I. INTRODUCTION

While inflationary cosmology is becoming a precision science, with the advent of recent and upcoming experiments such as the measurement of the cosmic microwave background radiation by the Planck satellite [1], the particle physics origin of inflatons still remains unclear. Because of their simplicity, single-field models of inflation are considered the most economical explanation of a Gaussian, nearly scale invariant spectrum of primordial fluctuations, as well as the flatness and the large-scale homogeneity of the observed Universe. Future experiments, however, could change this situation and put single-field models under pressure. For these reasons, there has been a keen interest in building multifield inflationary models, see e.g. the reviews [2,3]. Promising setups of multifield inflation include string-motivated models such as $\mathcal{N}$-flation [4], inflation from multiple M5-branes [5] and inflation from tachyons [6].

Naturally, the large parameter space for couplings, masses and initial conditions pertaining to multifield inflation makes a systematic analysis difficult. An interesting exception, nevertheless, is $\mathcal{N}$-flation. $\mathcal{N}$-flation is a string-motivated implementation of assisted inflation [7–12] where a large number of uncoupled scalar fields, identified with axions arising from Kachru, Kallosh, Linde and Trivedi (KKLT) compactification of type IIB string theory, assist each other to drive an inflationary phase [4]; see also [13–17]. One salient feature of this model is the possible avoidance of super-Planckian initial values. Further, using results from random matrix theory, the masses for the axion fields can be shown to conform to the Marčenko-Pastur (MP) law [13] under reasonable approximations. The spectrum of the masses is controlled by only two parameters, the average mass and a variable controlling the ratio between the number of axions and the total dimension of the moduli space. This renders $\mathcal{N}$-flation tractable despite the large number of fields. To a certain extent, successful inflation is contingent upon the initial conditions, however, the model becomes easily tractable by assuming that each field possesses equal initial energy.

Observable cosmological imprints from $\mathcal{N}$-flation have been computed by several groups. The tensor-to-scalar ratio r was calculated by Alabidi and Lyth [18] and was shown to have the same value as in the single-field case. The non-Gaussianity parameter f_{NL} was computed in [15,19] where the deviation from single-field models was found to be negligible. Unlike r and f_{NL}, the spectral index of the curvature perturbation n_s depends slightly on the model's parameters. References [13,15,16] showed that n_s is smaller (the spectrum being redder) than that found in single-field models, in agreement with the general discussion made in [20]. These results suggest that the observational data predicted by $\mathcal{N}$-flation are not drastically different from the single-inflaton case. Note however that the 5-year Wilkinson Microwave Anisotropy Probe (WMAP) data already exclude some region of the parameter space; see [21].

In this article, we study multifield preheating, focusing on $\mathcal{N}$-flation as a specific example. To our knowledge, a general theory of preheating for multifield inflationary models has not been fully developed. This is in part due to the highly nontrivial nature of the string theoretical constructions responsible for inflation. However, even at the phenomenological level, effects due to multiple inflatons contributing to preheating are largely unexplored in contrast to single-field inflation [22–26], see also [27–32]. For instance, preheating via parametric resonance of a matter field might be more efficient in the presence of multiple inflatons, as indicated in Cantor preheating [3,33]. Here, a nonperiodic variation of the matter field's effective mass leads to the dissolution of the stability bands and a possible parametric amplification of almost all

*diana.battefeld@helsinki.fi
+shinsuke.kawai@helsinki.fi

Fourier modes. This expectation is based on spectral theory [34–37], but a quantitative study about the magnitude of the amplification with more than two fields is missing [38]. Owing to the possible dissolution of the stability bands, one might expect that the collective behavior of the fields gives rise to efficient particle production after $\mathcal{N}$-flation.

To introduce the notation, let us consider a single-field model first: the equation of motion for a matter field χ_k with wave number k (assuming the coupling $g^2\varphi^2\chi^2/2$) can be written as a Mathieu equation [25],

$$\frac{d^2X_k}{d\tau^2} + [A - 2q\cos(2\tau)]X_k = 0, \tag{1}$$

for the comoving matter field $X_k = a^{3/2}\chi_k$, where $\tau = m_\varphi t$ is the rescaled time, m_φ the inflaton mass, and the two resonance parameters are

$$q = \frac{g^2\Phi_0^2}{4m_\varphi^2}, \qquad A = \frac{k^2}{a^2m_\varphi^2} + 2q. \tag{2}$$

Here, Φ_0 is the slowly varying inflaton amplitude, g is the inflaton-matter coupling and a the scale factor (see also Sec. IV). The efficiency of parametric resonance is controlled by the resonance parameter q, which needs to be large enough ($q \gg 1$) in order for the resonance effect to hold against cosmic expansion. The upper bound on the coupling constant g is given by the potential's stability condition against quantum gravity effects as well as radiative corrections [25,39] (unless the potential is protected by supersymmetry). This upper bound on g and $m_\varphi \sim 10^{-6}M_P$ (M_P is the reduced Planck mass) from the Cosmic Background Explorer (COBE) satellite normalization restricts the aforementioned resonance parameter q, leaving not much room for effective parametric resonance [39]. One might hope to alleviate this fine-tuning in multifield models.

For definiteness, we focus on $\mathcal{N}$-flation. We use the Marčenko-Pastur mass distribution for the axion masses, put forth in [13] based on random matrix theory, choosing the most likely mass distribution, see Sec. II. Further, for simplicity, we assume equal-energy initial conditions at the onset of inflation. Recently, aspects of preheating in the context of $\mathcal{N}$-flation have been considered in [40], pointing out the danger of transferring energy preferably to hidden sectors instead of standard model particles. This reveals an additional need for fine-tuning, a possible problem for many string-motivated models of inflation. The study in [40] is based entirely on an effective single-field description of $\mathcal{N}$-flation, such as the one above. Thus the common lore of parametric resonance models seems to be applicable in this work. Here we take the optimistic view that preheating might indeed occur in the visible sector. However, we go beyond the single-field model. We find that at the end of inflation more than 90% of the energy is confined to the lightest 10% of the fields in a very narrow mass range, while the remaining heavier fields are already more or less settled to the bottom of their potentials. Thus we focus on these lightest $\tilde{\mathcal{N}}$ fields during preheating. We also show that slow roll is indeed a good approximation, even though heavier fields violate the slow-roll condition $|\eta| < 1$ long before preheating starts. The initial values for preheating of the crucial $\tilde{\mathcal{N}}$ light fields are therefore given by their slow-roll values at the end of inflation. Since the lightest fields are highest up in their potentials, fields will join preheating in a staggered fashion. This and the still reasonably large number of fields makes a numerical treatment mandatory, which we provide. We solve the equations of motion for the matter field for various parameters following the above prescription and find that parametric resonance is less effective for $\mathcal{N}$-flation. The physical reason for the suppression of parametric resonance is the dephasing of the multiple fields. It is thus clear that effective single-field models fail to properly account for this effect. We conclude that the old theory of perturbative preheating, and not parametric resonance, is applicable when many fields of different masses couple to a single matter field.

This article is structured as follows: in Sec. II we review $\mathcal{N}$-flation and its dynamics during slow roll. We extend this discussion in Sec. III, where we provide an extrapolated slow-roll solution that slightly underestimates the inflatons' potential energy during inflation. We compare the slow-roll solution with a numerical solution and argue that even after $\eta < 1$ is violated by one or more of the heavier axion fields, the overall behavior of the inflatons is still well approximated by the slow-roll regime, up until preheating commences. In Sec. IV we set the stage for preheating corresponding to the end of slow roll for the effective single-field model. To begin, we set all axion masses equal to each other and discuss the physics of preheating in this particular system; then we return to $\mathcal{N}$-flation, where the Marčenko-Pastur mass spectrum is used. Finally, in Sec. V we conclude with comments and prospects for studying further issues on multifield preheating. In the Appendix we give a semianalytic solution that provides an upper bound for the inflaton potential, which further supports the observation made in Sec. III.

II. $\mathcal{N}$-FLATION AND SLOW ROLL

The action for $\mathcal{N}$ minimally coupled scalar fields, responsible for driving an inflationary phase, can be written as (see [2] for a review on multifield inflation)

$$S = -\int d^4x\sqrt{-g}\Big(\frac{1}{2}\sum_{i=1}^{\mathcal{N}} g^{\mu\nu}\nabla_\mu\varphi_i\nabla_\nu\varphi_i + W(\varphi_1, \varphi_2, \ldots)\Big), \tag{3}$$

where we assume canonical kinetic terms. The unperturbed volume expansion rate from an initial hypersurface at t_* to a final hypersurface at t_c (below we use $*$ and c to denote

values evaluated at t_* and t_c) is given by

$$N(t_c, t_*) \equiv \int_*^c H dt, \tag{4}$$

where N is the number of e-folds, H is the Hubble parameter and t is cosmic time.

In $\mathcal{N}$-flation [4], the $\mathcal{N}$ scalar fields that drive inflation are associated with axion fields. All cross couplings vanish when the periodic potentials are expanded around their minima [13]. Therefore, in the proximity of their minima the fields have a potential of the form

$$W(\varphi_1, \varphi_2, \ldots, \varphi_{\mathcal{N}}) = \sum_{i=1}^{\mathcal{N}} V_i(\varphi_i) = \sum_{i=1}^{\mathcal{N}} \frac{1}{2} m_i^2 \varphi_i^2, \tag{5}$$

where the fields have been arranged according to the magnitude of their masses, namely $m_i > m_j$ if $i > j$. $\mathcal{N}$-flation is a specific realization[1] of assisted inflation [7,9,43], where the $\mathcal{N}$ scalar fields assist each other in driving an inflationary phase. In this manner, individual fields do not need to traverse a super-Planckian stretch in field space. The spectrum of masses in (5), which were assumed to be equal in [4], can be evaluated by means of random matrix theory within a context of KKLT moduli stabilization [44], and was found by Easther and McAllister to conform to the MP law [13]. This results in a probability for a given square mass of

$$p(m^2) = \frac{1}{2\pi m^2 \beta \bar{m}^2} \sqrt{(m_{\max}^2 - m^2)(m^2 - m_{\min}^2)}, \tag{6}$$

where β and $\bar{m}^2$ completely describe the distribution. Here, $\bar{m}^2$ is the average mass squared and β controls the width and shape of the spectrum. The smallest and largest masses are given by

$$m_{\min} \equiv \bar{m}(1 - \sqrt{\beta}), \tag{7}$$

$$m_{\max} \equiv \bar{m}(1 + \sqrt{\beta}). \tag{8}$$

In this paper we split the mass range $(m_{\min}, m_{\max})$ into $\mathcal{N}$ bins,

$$(\tilde{m}_0, \tilde{m}_1), (\tilde{m}_1, \tilde{m}_2), \ldots, (\tilde{m}_{\mathcal{N}-1}, \tilde{m}_{\mathcal{N}}), \tag{9}$$

where $\tilde{m}_0 = m_{\min}$, $\tilde{m}_{\mathcal{N}} = m_{\max}$ and $\tilde{m}_{i-1} < \tilde{m}_i$, so that

$$\int_{\tilde{m}_{i-1}^2}^{\tilde{m}_i^2} p(m^2) dm^2 = \frac{1}{\mathcal{N}}, \qquad i = 1, 2, \ldots, \mathcal{N}. \tag{10}$$

We then represent each bin $(\tilde{m}_{i-1}, \tilde{m}_i)$ by an inflaton of mass m_i. In practice we simply set

$$m_i^2 = (\tilde{m}_{i-1}^2 + \tilde{m}_i^2)/2, \qquad i = 1, 2, \ldots, \mathcal{N}, \tag{11}$$

in the numerical computations. Apart from the $\mathcal{N}$ inflatons $\varphi_1, \varphi_2, \ldots, \varphi_{\mathcal{N}}$ with masses $m_1, m_2, \ldots, m_{\mathcal{N}}$, we introduce a fiducial inflaton φ_0 with mass $m_0 = m_{\min}$ for computational convenience (we shall use this as a clock). In [13], β is identified with the number of axions contributing to inflation divided by the total dimension of the moduli space (Kähler, complex structure and dilaton) in a given KKLT compactification of type IIB string theory. Because of constraints arising from the renormalization of Newton's constant [4] $\beta \sim 1/2$ is preferred. Hence, we will work with $\beta = 1/2$ in the following. Further, the magnitude of $\bar{m}$ is constrained by the COBE normalization [13,45], so that there is not much freedom in $\mathcal{N}$-flation to tune parameters.

At this point, we introduce a convenient dimensionless mass parameter

$$x_i \equiv \frac{m_i^2}{m_{\min}^2}, \tag{12}$$

as well as the suitable short-hand notation

$$\xi \equiv \frac{m_{\max}^2}{m_{\min}^2} = \left(\frac{1 + \sqrt{\beta}}{1 - \sqrt{\beta}}\right)^2. \tag{13}$$

A properly normalized probability distribution for the variable $x = m^2/m_{\min}^2$ is $\tilde{p}(x) = m_{\min}^2 p(m^2)$; hence expectation values with respect to the MP distribution can be evaluated via

$$\langle f(x) \rangle \equiv \frac{1}{\mathcal{N}} \sum_{i=1}^{\mathcal{N}} f(x_i) = \int_1^{\xi} \tilde{p}(x) f(x) dx = \frac{(1 - \sqrt{\beta})^2}{2\pi\beta} \int_1^{\xi} \sqrt{(\xi - x)(x - 1)} \frac{f(x)}{x} dx. \tag{14}$$

In Sec. III D and in the Appendix, we make use of the additional notation

$$\langle f(x) \rangle |_a^b \equiv \frac{(1 - \sqrt{\beta})^2}{2\pi\beta} \int_a^b \sqrt{(\xi - x)(x - 1)} \frac{f(x)}{x} dx, \tag{15}$$

where a and b are the limits of integration. When $f(x)$ is a polynomial in x, (14) reduces to a hypergeometric integral. In particular,

$$\langle x^{-1} \rangle = \xi^{-1/2}, \qquad \langle 1 \rangle = 1, \qquad \langle x \rangle = \frac{1}{(1 - \sqrt{\beta})^2}. \tag{16}$$

Figure 1 shows a plot of the probability distribution function $\tilde{p}(x)$, for $\beta = 1/2$.

Initially, we restrict ourselves to the slow-roll approximation. As we have already seen, $\mathcal{N}$ fields contribute to the energy density of the Universe through a separable potential. In this regime, the dynamics of $\mathcal{N}$-flation is as follows: first note that the field equations and Friedmann equations can be written as

[1]For a different realization of assisted inflation based on M-theory from multiple M5-branes, see [5,41]. See also [42] for another approach to random potentials in the landscape.

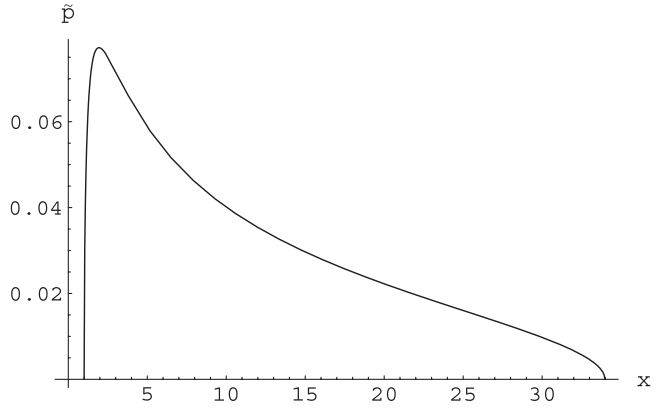

FIG. 1. A plot of the Marčenko-Pastur mass distribution over the dimensionless mass variable $x = m^2/m^2_{\rm min}$, for $\beta = 0.5$. Note that the MP distribution peaks in the small-mass region so that the majority of fields resides there. We use mass parameters $x_i = m_i^2/m^2_{\rm min}$ corresponding to the mass bins chosen according to (9)–(11), so that $x_0 \equiv 1 < x_1 < x_2 < \cdots < x_{\mathcal{N}-1} < x_{\mathcal{N}} < \xi \approx 34$.

$$3H\dot{\varphi}_i \approx -\frac{\partial V_i}{\partial \varphi_i} \equiv -V_i', \tag{17}$$

$$3H^2 \approx W. \tag{18}$$

Here and throughout most of our analysis, we set the reduced Planck mass to $M_P = (8\pi G)^{-1/2} \equiv 1$. The slow-roll approximation is valid if the parameters

$$\varepsilon_i \equiv \frac{1}{2}\frac{V_i'^2}{W^2}, \qquad \eta_i \equiv \frac{V_i''}{W}, \tag{19}$$

are small ($\varepsilon_i \ll 1$, $\eta_i \ll 1$) and

$$\varepsilon \equiv \sum_{i=1}^{\mathcal{N}} \varepsilon_i \ll 1 \tag{20}$$

holds. The number of e-folds of inflation becomes

$$N(t_c, t_*) = -\sum_{i=1}^{\mathcal{N}} \int_*^c \frac{V_i}{V_i'} d\varphi_i, \tag{21}$$

and the field equations can be integrated to yield

$$\left(\frac{\varphi_i^c}{\varphi_i^*}\right)^{1/m_i^2} = \left(\frac{\varphi_j^c}{\varphi_j^*}\right)^{1/m_j^2}. \tag{22}$$

Notice that this relationship between fields does not correspond to an attractor solution and predictions of $\mathcal{N}$-flation can depend on the initial conditions. Recall that we are assuming equal-energy initial conditions, namely $V_i^* = V_j^*$, which can be rewritten as

$$m_i\phi_i^* = m_j\phi_j^*. \tag{23}$$

A subtle feature of $\mathcal{N}$-flation is that if the mass spectrum is broad ($\xi \gg 1$, corresponding to $\beta \sim 1$), the heavier fields will acquire $\eta_i \approx 1$, even as inflation continues. This is the case even for the preferred value of $\beta \sim 1/2$, corresponding to $\xi \sim 34$. In the next section we show how to deal with $\mathcal{N}$-flation after $\eta_i \sim 1$ for the heaviest inflaton.

III. EVOLUTION OF INFLATONS AND AN EFFECTIVE SINGLE-FIELD MODEL DURING INFLATION

In this section we investigate the evolution of the axion fields after the slow-roll condition is violated for one or more of them. In order to study the system's collective behavior, it is useful to use an effective single-field description [2]. Given equal-energy initial conditions for the fields, the slow-roll parameter $\eta_{\mathcal{N}}$ of the heaviest field will be the first one to become of order unity [46]. Hence, prior to this moment we can safely implement an effective model composed of a single-field σ which evolves according to an effective potential $W_{\rm eff}(\sigma)$. After $\eta_{\mathcal{N}}$ became of order 1, the corresponding field $\varphi_{\mathcal{N}}$ cannot be described by the slow-roll solution. Below we argue that in our particular model of $\mathcal{N}$-flation the whole system is nevertheless well approximated by the slow-roll solution, up until the slow-roll parameter ε of (32) becomes of order 1[2]; during this stage, the contribution of the heavy axions is negligible compared to that of the lighter fields. This is due to three characteristic features of the model: (1) the majority of the axions is distributed around the lightest mass in the MP law; (2) the small value of the heaviest fields is prescribed by the equal-energy initial condition; hence, heavy fields provide a small contribution from the onset; (3) when the slow-roll condition $\eta_i < 1$ is violated for the heaviest fields the Hubble parameter is still very large, resulting in an overdamped evolution of the heavy fields.

Naturally, it is possible to continue using the slow-roll approximation when the next heaviest field violates slow roll and so on and so forth. This regime ends when slow roll fails for the effective single-field σ, after which light fields will actually start to evolve faster and preheating starts. It is important to note that we can trust our approximation up until preheating starts, where possible particle production due to nonlinear parametric resonance is our main concern.

A. Effective single-field model

Here we derive the effective single-field model based on the slow-roll approximation. This provides a lower bound to the evolution of the total potential energy. We identify the effective inflaton field σ as the path length of the trajectory in the $\mathcal{N}$ dimensional field space; namely, for $\mathcal{N}$ scalar fields ϕ_i we have [2]

[2]Or the slow-roll parameter of the effective degree of freedom in (32) becomes of order 1.

$$\sigma \equiv \int_{t_*}^{t} \sum_{i=1}^{\mathcal{N}} \hat{\sigma}_i \dot{\varphi}_i dt, \tag{24}$$

with

$$\hat{\sigma}_i \equiv \frac{\dot{\varphi}_i}{\sqrt{\sum_j \dot{\varphi}_j^2}}, \tag{25}$$

where the φ_i can be computed given the dynamical relations in (22), which are valid during slow roll, as well as the initial conditions in (23). Note that $\sigma = 0$ at the initial time t_*.

Using

$$y \equiv \frac{\varphi_0^2}{\varphi_0^{*2}} \tag{26}$$

(where y parameterizes how far the field φ_0 rolls down its potential) and x_i is defined in (12), as well as the equal-energy initial conditions (23), we can rewrite the dynamical relations as

$$\varphi_i^2 = \varphi_0^{*2} \frac{y^{x_i}}{x_i}. \tag{27}$$

We are using the fiducial inflaton φ_0 for computational convenience; φ_0 is not one of the $\mathcal{N}$ inflatons driving $\mathcal{N}$-flation (note that there is a vanishing probability for $m = m_0 = m_{\min}$ according to the MP law). From the Klein-Gordon equations during slow roll along with the Friedmann equation we obtain $\dot{\varphi}_i^2 = m_0^4 x_i \varphi_0^{*2} y^{x_i}/(3W)$, as well as $dy = -(2m_0^2 y/\sqrt{3W})dt$, with $W = (1/2)m_0^2 \varphi_0^{*2} \sum_{i=1}^{\mathcal{N}} y^{x_i}$. Using these relations in (24), we obtain an effective single-field solution (for which the subscript I is used),

$$\begin{aligned} \sigma_I(y) &= \frac{-\varphi_0^*}{2} \int_1^y \left(\sum_{i=1}^{\mathcal{N}} x_i s^{x_i} \right)^{1/2} \frac{ds}{s} \\ &= \frac{\sqrt{\mathcal{N}}}{2} \varphi_0^* \int_y^1 \sqrt{\langle x s^x \rangle} \frac{ds}{s}, \end{aligned} \tag{28}$$

where in the last step we used the definition of the MP-expectation values from (14) Similarly, the corresponding potential in (5) can be computed as

$$W_I(y) = \frac{1}{2} m_0^2 \varphi_0^{*2} \sum_{i=1}^{\mathcal{N}} y^{x_i} = \frac{\mathcal{N}}{2} m_0^2 \varphi_0^{*2} \langle y^x \rangle. \tag{29}$$

Equations (28) and (29) provide an implicit means of computing $W_I(\sigma_I)$. The number of e-folds can also be computed with this approximation. From (21) we find

$$N_I(y) = \frac{1}{4} \varphi_0^{*2} \sum_{i=1}^{\mathcal{N}} \left(\frac{1}{x_i} - \frac{y^{x_i}}{x_i} \right) = \frac{\mathcal{N}}{4} \varphi_0^{*2} [\langle x^{-1} \rangle - \langle x^{-1} y^x \rangle]. \tag{30}$$

Let us look at the solution more quantitatively. Since we would like to avoid super-Planckian initial conditions we assume the lightest possible inflaton to set off from the reduced Planck scale, $\varphi_0^* = 1$. Then it follows from the equal-energy initial conditions that all the other fields evolve safely within the sub-Planckian scale. Here and in the following we use the preferred $\beta = 1/2$ so that the ratio of the heaviest to the lightest mass squared in (13) is about $\xi \approx 34$. The e-folding number (30) depends linearly on the number of inflatons $\mathcal{N}$. If we take $\mathcal{N} = 1500$ we get $N_{\max} \equiv N_I(0) \approx 64.3$, which is large enough to solve the standard cosmological problems. Note, however, that one cannot trust (28) and (29) down to $y = 0$, since slow roll ends earlier. Strictly speaking, our effective single-field solution (with subscripts I) is only valid as long as the slow-roll conditions are satisfied, that is until $\eta_{\mathcal{N}} = 1$. Using (29) and $m_{\mathcal{N}} \approx m_{\max}$ this can be written as

$$\langle y^x \rangle = \frac{2\xi}{\mathcal{N} \varphi_0^{*2}}, \tag{31}$$

from which the value of y at $\eta_{\mathcal{N}} = 1$ is found numerically as $y_{\mathcal{N}} \approx 0.488$ for $\mathcal{N} = 1500$. The number of e-folds at this instant is $N_I(y_{\mathcal{N}}) \approx 55.6$ and we see that there is still a breadth of inflation to come. If we ignore this fact, we could extrapolate σ_I up until this effective degree of freedom leaves its own slow rolling regime when

$$\epsilon_\sigma \equiv \frac{1}{2} \left(\frac{W_I'}{W_I} \right)^2 = 1. \tag{32}$$

This equation can be rewritten as

$$2\langle x y^x \rangle = \mathcal{N} \varphi_0^{*2} \langle y^x \rangle^2, \tag{33}$$

where we used

$$\begin{aligned} W_I' \equiv \frac{\partial W_I}{\partial \sigma_I} &= \sum_{i=1}^{\mathcal{N}} \hat{\sigma}_i \frac{\partial V_i}{\partial \varphi_i} = \sum_{i=1}^{\mathcal{N}} \hat{\sigma}_i m_i^2 \varphi_i \\ &= m_0^2 \varphi_0^* \sqrt{\mathcal{N} \langle x y^x \rangle}. \end{aligned} \tag{34}$$

Equation (33) can be numerically solved to obtain $y_{\text{end}} \approx 0.0836$ for $\mathcal{N} = 1500$ so that $\sigma_I(y_{\text{end}}) \approx 17.6$ and $N_I(y_{\text{end}}) \approx 63.8$. At this point inflation comes to an end and preheating is about to commence. The potential at this instant is $W_I(y_{\text{end}}) \approx 0.128 \bar{m}^2 \approx 1.49 m_0^2$ (see Table I).

B. Implications for non-Gaussianities

In contrast to single-field inflationary models, in which non-Gaussianities (NG) are known to be suppressed, in multifield models there is a possibility that NG may become large due to the existence of isocurvature perturbations [47]; if there is a sudden turn of the trajectory in field space as in the case of the curvaton scenario, a conversion of isocurvature perturbations into adiabatic ones takes place, giving rise to larger NG. In $\mathcal{N}$-flation the nonline-

arity parameters characterizing the bi- and trispectrum were investigated in the horizon crossing approximations in [19] and it was found that $\mathcal{N}$-flation is indistinguishable from single-field inflationary models in this limit. Also, incorporating the evolution of perturbations after horizon crossing, but still within slow roll, revealed that additional contributions remain negligible [19]. Hence, NG are expected to be heavily suppressed as long as slow roll is considered [46]. In the present paper we investigate the evolution in $\mathcal{N}$-flation after the slow-roll condition is violated for one or more of the axion fields and find (see the next sections) that the extrapolated slow-roll solution remains a good approximation up until preheating commences. Thus, in this intermediate regime (after slow-roll inflation but before preheating), NG should also be suppressed; additional NG would be due to the evolution of the adiabatic mode after horizon crossing; for this to occur, isocurvature modes have to source the adiabatic one, but in $\mathcal{N}$-flation, the trajectory in field space is smooth; therefore, NG should be heavily suppressed up until slow roll fails for the effective single degree of freedom, i.e. when preheating begins. During preheating NG may still appear; this requires further study, and we hope to come back to this issue in the near future.

C. Numerical solutions

Figure 2 shows the time evolution of $\mathcal{N} = 1500$ axions in our setup, namely, the MP mass distribution with $\beta = 0.5$ and the equal-energy initial conditions, obtained numerically. The plot shows φ_i with $i = 1$, 300, 600, 900, 1200 and 1500. For the initial conditions we used (23) with $\varphi_0^* = 1$ and $\dot{\varphi}_i^* = 0$. Because of these initial values, lighter axions evolve from larger values, closer to 1. The figure clearly shows that heavy axions, even φ_{300}, roll down the potential rapidly and their oscillation amplitudes are much smaller than that of the lightest field φ_1. Indeed, fields are usually overdamped up until preheating starts. Naturally, the lighter fields are expected to be responsible for preheating (unless the coupling between the heavy fields and a matter field is extremely strong).

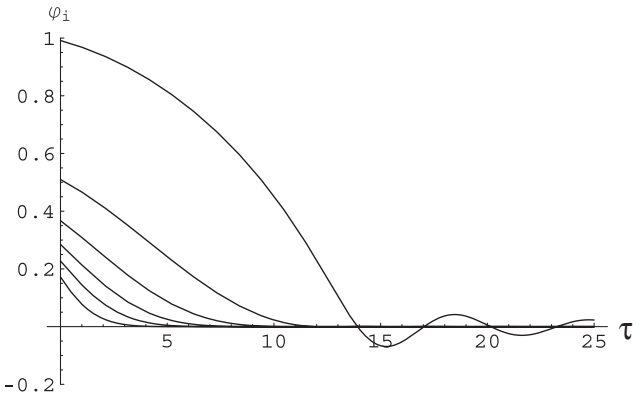

FIG. 2. Evolution of the axion fields for $\mathcal{N} = 1500$ (numerical result). The figure shows φ_i with $i = 1$, 300, 600, 900, 1200, 1500 from the top. The time $\tau = m_0 t$ is in units measured by the fiducial mass $m_0 = m_{\rm min}$. In this unit, $y = y_{\mathcal{N}}$ is at $\tau = 7.14$ and $y = y_{\rm end}$ is at $\tau = 11.6$.

In Table I we summarize the values of W and N obtained by the extrapolated slow-roll solutions (I) and numerical results, at $\sigma = \sigma(y_{\mathcal{N}})$ and $\sigma(y_{\rm end})$. A comparison between the analytic and numerical computation for $\mathcal{N} = 100$, 200, 400, 1500 reveals an agreement, roughly within 15%, indicating that the extrapolated slow-roll solution (I) is a good approximation up until $y_{\rm end}$. In the Appendix we provide a semianalytic computation of an upper bound to W (solution II), which further supports this observation. How many inflatons still satisfy the slow-roll condition $\eta_i < 1$ at $y_{\rm end}$? This can be found by comparing the values of $W(y_{\rm end})/m_0^2$ and the mass parameter x_i, since $\eta_i = m_i^2/W = x_i m_0^2/W$. Numerically, we find that 13, 18, 25, 56 lightest fields are still in the slow-roll regime at $y = y_{\rm end}$, for $\mathcal{N} = 100$, 200, 400, 1500. Analytically, solution

TABLE I. Comparison of analytic and numerical solutions for the effective single-field values W and N at $\sigma(y_{\mathcal{N}})$ and $\sigma(y_{\rm end})$, for the number of inflatons $\mathcal{N} = 100$, 200, 400, and 1500. The values of σ_I are found using (28) and the corresponding analytic and numerical values for W/m_0^2 and N are shown. Apart from the conspicuous disagreement in the e-folding number N for small $\mathcal{N}$, the extrapolated slow-roll solutions (I) are relatively in good agreement with the numerical solutions, roughly within 15% difference. Typically, the results of solution (I) slightly underestimate the potential W.

		Solution I			Numerical	
$\mathcal{N}$	$y_{\mathcal{N}}$ / $y_{\rm end}$	$\sigma_I(y_{\mathcal{N}})$ / $\sigma_I(y_{\rm end})$	$W_I(y_{\mathcal{N}})$ / $W_I(y_{\rm end})$	$N_I(y_{\mathcal{N}})$ / $N_I(y_{\rm end})$	$W(y_{\mathcal{N}})$ / $W(y_{\rm end})$	$N(y_{\mathcal{N}})$ / $N(y_{\rm end})$
100	0.964	0.541	34.0	0.758	34.0	1.10
	0.502	3.27	2.43	3.67	2.83	4.34
200	0.879	2.00	34.0	3.72	34.3	4.14
	0.331	5.40	1.97	8.00	2.27	8.83
400	0.762	4.37	34.0	10.9	34.4	11.4
	0.211	8.33	1.73	16.6	1.95	17.6
1500	0.488	12.86	34.0	55.6	34.4	56.3
	0.0836	17.61	1.49	63.8	1.62	65.1

I yields somewhat smaller values: 10, 13, 18, 41, respectively.

D. Light axion dominance

From Fig. 2 we can infer that heavy fields lose energy quite rapidly and that the later stage of $\mathcal{N}$-flation is driven solely by the light fields. To see this quantitatively let us introduce the ratio of the potential energy of ℓ lightest fields to that of all $\mathcal{N}$ fields, defined by

$$R_\ell \equiv \frac{W_{\rm light}}{W_{\rm total}} = \frac{\sum_{i=1}^{\ell} V_i}{\sum_{i=1}^{\mathcal{N}} V_i}. \tag{35}$$

Using the extrapolated slow-roll solution (I), this ratio can be evaluated as

$$R_\ell^I(y) = \frac{\sum_{i=1}^{\ell}\langle y^{x_i}\rangle}{\sum_{i=1}^{\mathcal{N}}\langle y^{x_i}\rangle} = \frac{\langle y^x\rangle|_1^{\tilde{x}_\ell}}{\langle y^x\rangle}. \tag{36}$$

The ratio of the number of light fields to all fields is similarly

$$\lambda \equiv \frac{\ell}{\mathcal{N}} = \langle 1\rangle|_1^{\tilde{x}_\ell}. \tag{37}$$

Figure 3 shows $R_\ell^I(y)$ versus λ and y. Note that this plot does not depend on $\mathcal{N}$ (however $y_{\mathcal{N}}$ and $y_{\rm end}$ do depend on $\mathcal{N}$). For small y (i.e. at late time), R_ℓ^I approaches 1 for

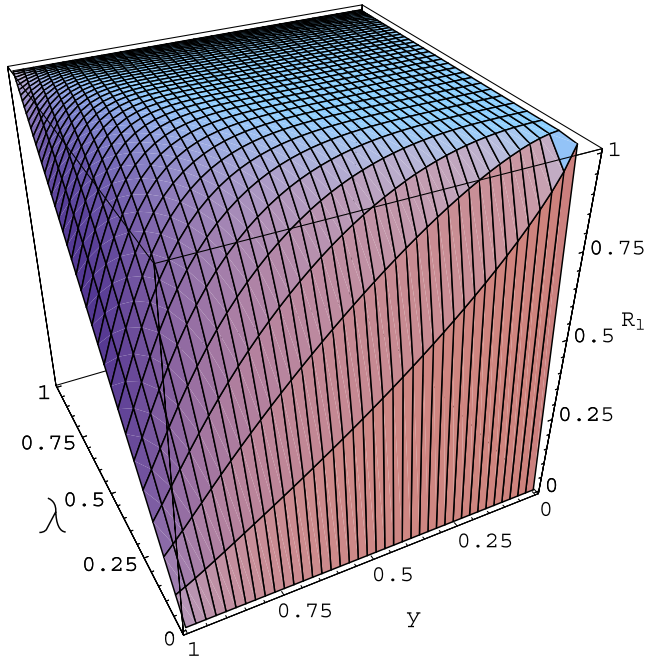

FIG. 3 (color online). The ratio of potential energies of the light fields to all axions, R_ℓ^I, is plotted against $\lambda = \ell/\mathcal{N}$ and y. The figure does not depend on $\mathcal{N}$. Note that in calculating R_ℓ^I we are using the slow-roll approximation which is not reliable after $y_{\rm end}$. For larger $\mathcal{N}$, the value of $y_{\rm end}$ tends to be smaller, and hence the domination of light axions tends to be stronger.

TABLE II. The ratio of the potential energy carried by the lightest axions (10%) with respect to the total potential energy, evaluated at the end of slow-roll regime $\sigma = \sigma(y_{\rm end})$. The table shows both semianalytic and numerical results.

$\mathcal{N}$	Solution I	Numerical
100	62.9	63.3
200	78.4	80.0
400	88.0	89.9
1500	96.5	97.5

even small values of λ, indicating that the potential energy is dominated by light axions.

Table II summarizes the amount of the total potential energy carried by the lightest 10% of the axions at $\sigma = \sigma(y_{\rm end})$, for $\mathcal{N} = 100, 200, 400, 1500$. These values are calculated using both, solution I and numerical computations. The results clearly show that for large $\mathcal{N}$, the potential energy is carried by only a small portion of lightest axion fields. Using (36), it is not difficult to check that this tendency becomes stronger when $\mathcal{N}$ is larger. This in turn justifies our usage of the approximation given by solution I, which corresponds to using slow roll for all fields, even if the slow-roll condition $\eta_i < 1$ is violated for the majority of fields; all in all, heavy fields do not contribute much to the total potential energy, and henceforth inflation.

IV. PREHEATING

Now let us discuss the physics of preheating. In order to solve problems of the standard big-bang cosmology the number of e-foldings must be large enough; with this in mind, we assume $\mathcal{N} = 1500$ in the following. If we forget about its string theoretical origin (which we do in this paper), $\mathcal{N}$ can be even larger, giving rise to a (harmless) larger number of e-folds. Our choice of $\mathcal{N}$ is for definiteness, and also for numerical tractability.

A. The model of preheating

We first recall that the axion mass scale is observationally constrained. The power spectrum for multifield models is computed by the δN-formalism [48] and for $\mathcal{N}$-flation it becomes [13,45]

$$\mathcal{P}_{\mathcal{R}} = \sum_i \frac{m_i^2\varphi_i^2}{96\pi^2 M_P^6}\sum_j \varphi_j^2 = \frac{\mathcal{N}^2 m_0^2 \varphi_0^{*4}}{96\pi^2 M_P^6}\langle y^x\rangle\langle x^{-1}y^x\rangle, \tag{38}$$

where in the second line the MP distribution and equal-energy initial conditions have been used. To be specific, if we evaluate $\mathcal{P}_{\mathcal{R}}$ at $t = t_*$ (corresponding to large scales) we obtain

$$\mathcal{P}_{\mathcal{R}} = \frac{\mathcal{N}^2 m_0^2 \varphi_0^{*4}}{96\pi^2 M_P^6}\langle x^{-1}\rangle. \tag{39}$$

Comparing this with $\mathcal{P}_{\mathcal{R}} \approx 2.3 \times 10^{-9}$ from WMAP measurements [49–51], we find the mass of the lightest field

$$m_0 \approx 2.4 \times 10^{-6} M_P, \tag{40}$$

for $\mathcal{N} = 1500$, $\beta = 0.5$ and $\varphi_0^* = M_P$. Consequently, the average mass is $\bar{m} = m_0/(1 - \sqrt{\beta}) \approx 8.1 \times 10^{-6} M_P$. In what follows, we assume these values for the mass parameters; all other masses follow via the MP distribution.

In the previous section we have seen that the late stage of $\mathcal{N}$-flation is mainly driven by a few light axions; we naturally expect that preheating is triggered by these lightest axions, coupled to a matter field, at least before backreaction becomes important. Thus, in this section we focus on the relevant $\tilde{\mathcal{N}} = 150$ light axions, which carry more than 95% of the total potential energy at $y = y_{\text{end}}$. It is important to note at this point that the relevant mass scale for preheating is set by the mass of the light fields and not the average mass $\bar{m}$. For the matter into which the inflatons decay, we consider a massless bosonic field χ coupled to the axions via the coupling $\frac{1}{2} g^2 \varphi_i^2 \chi^2$, where we assume for simplicity an identical coupling constant to each φ_i. The model we consider is then described by the following Lagrangian:

$$\mathcal{L} = -\sum_{i=1}^{\tilde{\mathcal{N}}}\left\{\frac{1}{2} g^{\mu\nu}\nabla_\mu\varphi_i\nabla_\nu\varphi_i + \frac{1}{2} m_i^2\varphi_i^2 + \frac{1}{2} g^2\varphi_i^2\chi^2\right\} - \frac{1}{2} g^{\mu\nu}\nabla_\mu\chi\nabla_\nu\chi. \tag{41}$$

The equations of motion are

$$\ddot{\varphi}_i + 3H\dot{\varphi}_i + (m_i^2 + g^2\langle\chi^2\rangle)\varphi_i = 0, \tag{42}$$

$$\ddot{\chi}_k + 3H\dot{\chi}_k + \left(\frac{k^2}{a^2} + g^2\sum_i \varphi_i^2\right)\chi_k = 0, \tag{43}$$

$$3H^2 = \frac{1}{2}\sum_i \dot{\varphi}_i^2 + \frac{1}{2}\sum_i m_i^2\varphi_i^2 + \frac{1}{2}\langle\dot{\chi}^2\rangle + \frac{1}{2} g^2\langle\chi^2\rangle\sum_i \varphi_i^2, \tag{44}$$

where χ_k is the mode operator of the matter field and $\langle\cdot\rangle$ is the mode sum over k. We consider the axions and gravity as the background, and ignore backreaction from the matter field χ_k; consequently, $\langle\chi^2\rangle$ and $\langle\dot{\chi}^2\rangle$ are set to zero.

B. Parametric resonance in the equal-mass case

Before addressing the more involved preheating scenario of $\mathcal{N}$-flation, we discuss a model with $\tilde{\mathcal{N}} = 150$ inflatons having the same mass, $m_i \equiv m$.

In this case, the equal-energy initial conditions set the same initial values for all $\tilde{\mathcal{N}}$ axions, so that the evolution of the $\tilde{\mathcal{N}}$ axions is identical. Neglecting backreaction of the matter field we can write the equations of motion as

$$\begin{aligned} &\ddot{\varphi}_i + 3H\dot{\varphi}_i + m^2\varphi_i = 0, \\ &\ddot{\chi}_k + 3H\dot{\chi}_k + \left(\frac{k^2}{a^2} + \tilde{\mathcal{N}} g^2\varphi_i^2\right)\chi_k = 0, \\ &3H^2 = \frac{\tilde{\mathcal{N}}}{2}(\dot{\varphi}_i^2 + m^2\varphi_i^2). \end{aligned} \tag{45}$$

Defining $\varphi \equiv \sqrt{\tilde{\mathcal{N}}}\varphi_i$, the equations of motion reduce to those of the well-understood single-field model, yielding nonperturbative preheating [3,23–25,52]. The Klein-Gordon equation for φ reads

$$\ddot{\varphi} + 3H\dot{\varphi} = -m^2\varphi, \tag{46}$$

whose solution is approximated during the preheating era by

$$\varphi(t) = \Phi(t)\sin(mt), \tag{47}$$

where $\Phi(t) = \sqrt{8}/(\sqrt{3}mt)$ [25] is a slowly decaying amplitude due to Hubble friction. The corresponding equation for a Fourier mode of the matter field reads

$$\ddot{\chi}_k + 3H\dot{\chi}_k + \left(\frac{k^2}{a^2} + g^2\varphi^2\right)\chi_k = 0, \tag{48}$$

where $\mathbf{p} = \mathbf{k}/a$ is the physical momentum. Because of the oscillations of the inflaton field, the mass of the matter field becomes time dependent and resonances can occur. To see this, introduce $q = g^2\Phi^2/4m^2$, $\tau = mt$, $A_k = 2q + k^2/m^2a^2$ and $X_k \equiv a^{3/2}\chi_k$ so that (48) becomes

$$\frac{d^2X_k}{d\tau^2} + (A_k - 2q\cos(2\tau))X_k = 0, \tag{49}$$

where we also neglected the term proportional to the pressure, $-(3/4)(H^2 + 2\ddot{a}/a)$. If we ignore the time dependence of the amplitude Φ in q and of A_k, Eq. (49) is the Mathieu equation. It is known that parametric resonance occurs for wave numbers k within resonance bands (see [25,53] for the stability/instability chart). This means if k is within the nth resonance band, the corresponding mode increases exponentially

$$X_k \propto e^{\mu_k^{(n)}\tau}, \tag{50}$$

where $\mu_k^{(n)} > 0$ is the Floquet index [53]. Physical parameters correspond to the region $A_k \geq 2q$ and, in particular, the zero mode $k = 0$ evolves along the $A_k = 2q$ line from large q to $q \sim 0$, as the inflaton amplitude Φ decays slowly. As it evolves, the system crosses resonance bands where exponential particle production takes place. Particle production is efficient in the large q ($q \gg 1$) region, *broad resonance* (or *stochastic resonance* when expansion effects are included). For small q the resonance effect is limited as it is not strong enough to hold against redshifting $\chi_k \propto a^{-3/2}$. Then the main concern is whether it is possible to

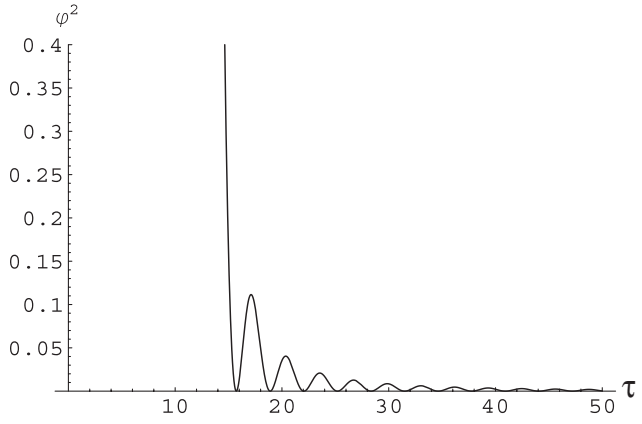

FIG. 4. The evolution of the oscillating term φ^2 that drives parametric resonance. The horizontal axis is the dimensionless time $\tau = m_0 t$. Since $\varphi = \sqrt{\tilde{\mathcal{N}}}\varphi_i$ and φ_i are chosen to start from $M_P = 1$, φ^2 starts from $\tilde{\mathcal{N}} = 150$ at $\tau = 0$.

have a large enough q in a given model. A stringent constraint comes from radiative corrections, restricting the value of the coupling to $g \lesssim 10^{-3}$ [25,39].

From the above discussion it can be deduced that having many inflatons does not increase q, and resonance effects are not enhanced. Given that the equations of motion lead to the one of the single-field model, $\varphi(=\sqrt{\tilde{\mathcal{N}}}\varphi_i)$ starts oscillating from the single-field value $\sim 0.2 M_P$. Each inflaton φ_i oscillates with smaller amplitude $\Phi/\sqrt{\tilde{\mathcal{N}}}$, while q is unaltered. In the next subsection, we compare the equal-mass case to a broader mass distribution (MP mass distribution). To this aim, we provide numerical plots. In Fig. 4, we show the evolution of the oscillating term φ^2 in the equal-mass case, where we have chosen $\tilde{\mathcal{N}} = 150$, $m = m_0 = 2.4 \times 10^{-6} M_P$. The initial values of φ_i are all taken to be $M_P = 1$, and the initial velocities are $\dot{\varphi}_i = 0$. In Fig. 5 the evolution of the matter field mode function χ_k and the comoving occupation number of particles, defined by

$$n_k = \frac{1}{2}\left(\frac{|\dot{X}_k|^2}{\omega_k} + \omega_k |X_k|^2\right) - \frac{1}{2}, \tag{51}$$

are shown for $g = 10^{-3}$ and $k/a_{\rm init} = 6.0 \times m$ (corresponding to a fastest growing mode, see [25]). Here,

$$\omega_k = \sqrt{\frac{k^2}{a^2} + g^2 \sum_i \varphi_i^2}, \tag{52}$$

which reduces to $\sqrt{k^2/a^2 + g^2\varphi^2}$ in the present case. The condition on the resonance parameter $q = g^2\Phi^2/4m^2 \gtrsim \mathcal{O}(1)$ corresponds to $|\varphi|^2 \gtrsim 10^{-5}$ for $g = 10^{-3}$, which is roughly $\tau \lesssim 4000$. We are ignoring both, backreaction and rescattering effects. The corresponding plots for the Marčenko-Pastur distribution are shown in Figs. 6 and 10 below.

C. Numerical results for the Marčenko-Pastur case

Let us turn to the question of multiple fields whose masses obey the MP law. The equations of motion of our system are (42)–(44); we are assuming that all inflaton fields are coupled to the same matter field with identical strength g^2, and we consider only $\tilde{\mathcal{N}} = 150$ axions since the heavier 90% of the axions are negligible in the later stage of $\mathcal{N}$-flation. We also ignore backreaction, meaning we set $\langle\chi^2\rangle = \langle\dot{\chi}^2\rangle = 0$ (which, in the end, is justified since amplification of the matter field is found to be suppressed). The initial values and the velocities of the axions at the onset of preheating $y = y_{\rm end}$ correspond to the extrapolated slow-roll solution, discussed in Sec. III:

$$\varphi_i(y_{\rm end}) = \varphi_0^* \sqrt{\frac{y_{\rm end}^{x_i}}{x_i}}, \tag{53}$$

$$\dot{\varphi}_i(y_{\rm end}) = -m_0^2 \varphi_0^* \sqrt{\frac{x_i y_{\rm end}^{x_i}}{3W_I(y_{\rm end})}}. \tag{54}$$

The initial conditions for the matter field are set by the

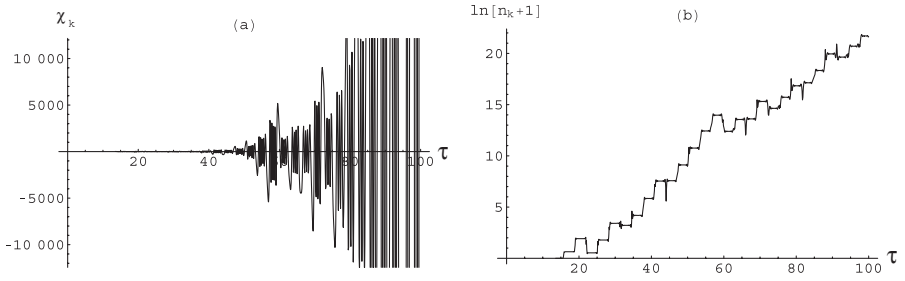

FIG. 5. The evolution of (the real part of) the mode χ_k (a) and the occupation number n_k (b). The initial conditions for χ_k are set by the positive-frequency solution at $\tau = 13.5$, when the slow-roll conditions break down. The coupling constant is $g = 10^{-3}$ and the wave number is chosen as $k/am = 6.0$ at $\tau = 13.5$. One can see amplification due to typical stochastic resonance, i.e. the overall amplitude grows exponentially while there are occasional decreases of the amplitude. We are ignoring backreaction so that resonances are present until $q \approx \mathcal{O}(1)$, corresponding to $\tau \approx 4000$ for $g = 10^{-3}$. Backreaction from the matter field shuts off resonances earlier.

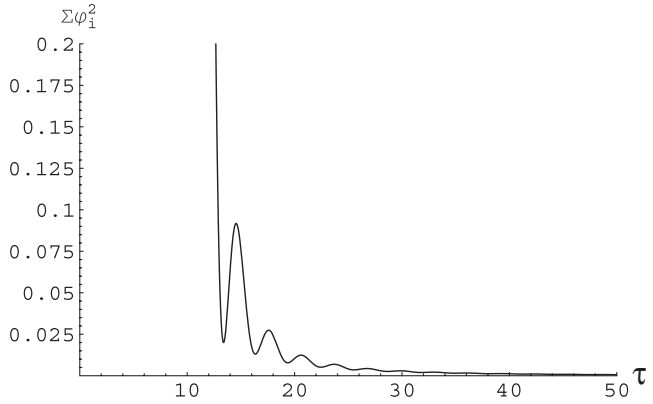

FIG. 6. The evolution of the term $\sum_i \varphi_i^2$ that couples to the matter field. The time is as in Fig. 2. Oscillations are less sharp than in the equal-mass case, Fig. 4.

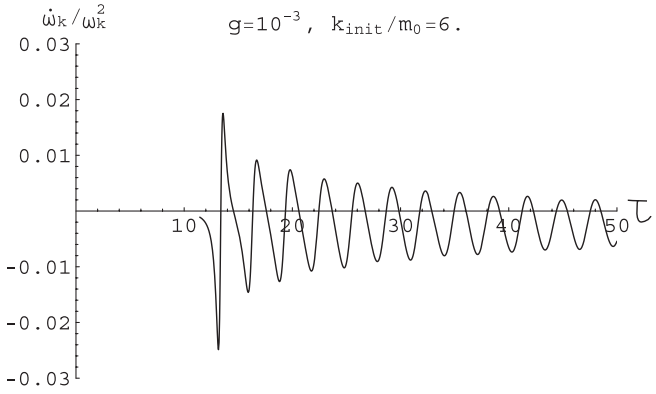

FIG. 8. The adiabaticity parameter $\dot\omega_k/\omega_k^2$, for $\tau \lesssim 50$. The slight negative shift is due to the cosmic expansion.

positive-frequency mode function, $X_k(t) = a^{3/2}\chi_k(t) \simeq e^{-i\omega_k(t-\tau_{\rm end}/m_0)}/\sqrt{2\omega_k}$, at $\tau = \tau_{\rm end} = 11.6$ corresponding to the onset of the preheating stage $y = y_{\rm end}$.

Short time scale behavior: Fig. 6 shows the evolution of $\sum_i \varphi_i^2$ until $\tau = 50$. The horizontal axis used here is the dimensionless time $\tau = m_0 t$. Clearly, the axion masses are all different in the Marčenko-Pastur case, resulting in a somewhat different evolution of the $\sum_i \varphi_i^2$ term from the equal-mass case. We can see that the oscillations are more obtuse compared to Fig. 4; this is a consequence of dephasing of the axion oscillations owed to relative mass differences. As the time-dependent mass term oscillates, some resonance effects for the dynamics of χ_k are expected. This is indeed the case, at least to some extent. Figure 7(a) shows the time evolution of the matter field mode function ($g = 10^{-3}$ and $k/am_0 = 6.0$ at $\tau = \tau_{\rm end}$, as in the previous section). The temporal enhancement of the amplitude (which is clearly seen for small τ but becomes weaker for large τ) is caused by parametric resonance with (the collective behavior of) the axions. In contrast to the equal-mass case, the amplitude of χ_k decreases on average; the resonance effect is not strong enough to resist dilution due to cosmic expansion, even when the coupling constant is as large as $g \sim 10^{-3}$.

One can separate out the effect of cosmic expansion by looking at the comoving field $X_k = a^{3/2}\chi_k$. The equation of motion for X_k is

$$\ddot{X}_k + \left[\frac{k^2}{a^2} + g^2\sum_i \varphi_i^2 - \frac{3}{4}(2\dot{H} + 3H^2)\right]X_k = 0, \quad (55)$$

where the last term in the square bracket is proportional to the pressure and is very small during reheating. Figure 7(b) shows the numerical plot of the evolution of X_k. We can see that the peaks occur when $\sum_i \varphi_i^2$ of Fig. 6 reaches local minima, and $\dot\omega_k/\omega_k^2$ becomes large (see Fig. 8), i.e. when the system becomes less adiabatic; this is characteristic of parametric resonance. In contrast to the equal-mass case, the minima of the mass term do not approach zero due to dephasing, caused by the relative mass differences of the axion fields. This yields relatively small $\dot\omega_k/\omega_k^2$ and makes preheating inefficient.

One can see that the amplitude of X_k exhibits power-law–like growth on average. This growth does not necessarily mean production of particles, since it is mainly due to redshift [25]. When k is large the power $X_k \sim a^\gamma$ tends to

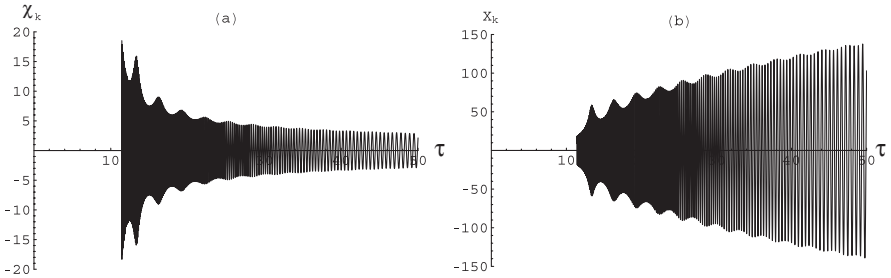

FIG. 7. (a) The evolution of the mode function of the matter field χ_k, in $\mathcal{N}$-flation using the MP mass distribution. The coupling is $g = 10^{-3}$ and the wave number is chosen as $k/am_0 = 6.0$ at $\tau = \tau_{\rm end} = 11.6$. (b) The evolution of $X_k = a^{3/2}\chi_k$ for the same parameters. There are wiggles in the oscillation amplitude (these are evident for small τ and become smaller for larger times) indicating some effect of parametric resonance. This resonance is, however, not strong enough and the amplitude of χ_k decays on average.

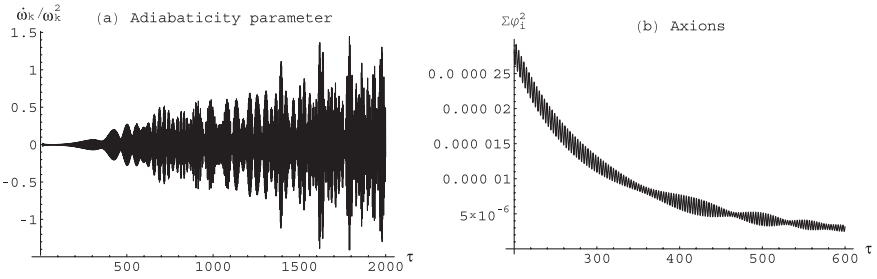

FIG. 9. (a) The long time scale behavior of the adiabaticity parameter $\dot{\omega}_k/\omega_k^2$. (b) The sum of axions' squared amplitudes $\sum_i \varphi_i^2$, for the time scale $\tau = 200$ to 600. The coupling g and the wave number k are the same as in Fig. 7.

$\gamma \approx 0.5$, which is understood as follows: in the mass term of (55), k^2/a^2 is dominant and it stays dominant since $a^{-2} \sim t^{-4/3}$, $\varphi_i^2 \sim t^{-2}$, $\dot{H} \sim t^{-2}$ and $H^2 \sim t^{-2}$ as $a \sim t^{2/3}$ during preheating. Then (55) becomes $\ddot{X}_k + Ct^{-4/3}X_k = 0$ for some constant C, which is exactly soluble in the form of $X_k \sim t^\alpha F(t)$ where $F(t)$ is a fast oscillating function; discarding the decaying solution we find $\gamma = 3\alpha/2 = 0.5$. For smaller k, X_k grows faster than $\sim a^{0.5}$; for $k \approx 0$ we find $\sim a^{0.75}$ numerically.

Long time scale behavior: In the equal-mass model (see Sec. IV B), with a large enough value of g, the resonance parameter is $q \gg 1$ and resonances arise for reasonably long time scales, specifically, up until $\tau \approx 4000$ for $g = 10^{-3}$ (ignoring backreaction). Similarly, in the MP case, even though there is no well-defined q-parameter, resonances can ensue during short time intervals for large τ, again assuming a similar large coupling g. In this case, the collective behavior of the axions is crucial and the adiabaticity parameter $\dot{\omega}_k/\omega_k^2$ shows a rather complicated behavior [see Fig. 9(a)]. Since the mass differences between the neighboring axions in (11) with $\mathcal{N} = 1500$ is typically of order of $\Delta m^2 \approx \mathcal{O}(10^{-2}) \times m_0^2$, once dephased, the axions' collective oscillations return to near coherence in time scales of order $\Delta\tau \approx \mathcal{O}(10^2)$, causing beats in the effective mass for χ_k [see Fig. 9(b)]. In Fig. 10 we show the evolution of χ_k until $\tau = 2000$ [Fig. 10(a)], and the evolution of the comoving occupation number n_k calculated for X_k [Fig. 10(b)]. In this example, there is some amplification due to parametric resonances around $\tau \approx 450$. On these time scales, for $g \gtrsim 10^{-3}$ and small k, we find the occasional amplitude enhancement of a few orders of magnitude. For larger wave numbers ($k/am_0 \gtrsim 10^4$ at $\tau = \tau_{\rm end}$) we find somewhat different behavior of n_k. The overall amplitude of $\dot{\omega}_k/\omega_k^2$ becomes smaller but the spikes at large τ remain. Consequently, the bursts at $\tau \approx 450$ disappear and the late time dynamics is dominated by a random-walk–like behavior. These resonance effects are, however, not frequent or long enough to dominate preheating.

To summarize, we saw that preheating of a single matter field is not due to explosive particle production in $\mathcal{N}$-flation; even though there is some amplification, it is too weak in small time scales and not very frequent in large time scales, to compete with the dilution due to Hubble expansion. We have also studied parameters not presented above, including larger values of the coupling g; for $g = 3 \times 10^{-3}$ the resonance is barely sufficient to compete with the Hubble expansion. For the MP parameter $\beta = 0.7$ and 0.9, we found similar results (inefficient resonance). The physical reason for the suppression of parametric resonance can be understood as follows: the axions are all out of phase, averaging out each other's contribution, so that the driving term $\propto \sum \varphi_i^2$ in the equation of motion for χ_k does not provide a coherent oscillatory behavior that is needed for efficient parametric resonance. Hence, instead of an exponential increase, we observe power-law–like behavior $\chi_k \sim a^{\gamma-3/2}$ in time scales $\tau \lesssim 200$, where γ is typically between 0.5 and 0.75 for the parameter region we

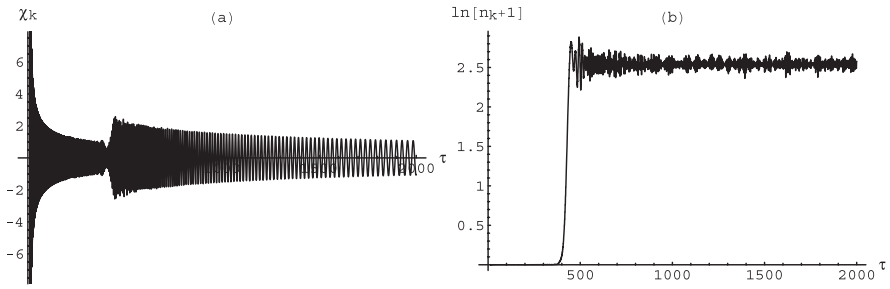

FIG. 10. (a) Long time behavior of χ_k, exhibiting short-lived, weak resonances around $\tau \approx 450$. The choice of parameters is the same as in Fig. 7. (b) The comoving occupation number n_k calculated for X_k.

have studied. For longer time scales $\tau \approx 200$–2000, we find occasional particle production, although these are not strong enough to dominate preheating. This conclusion differs from the common lore, namely, that parametric resonance effects are crucial for preheating [3].

V. CONCLUSIONS

In this paper we studied the late time dynamics of $\mathcal{N}$-flation, a string-motivated realization of assisted inflation, assuming the Marčenko-Pastur mass distribution (arising from random matrix theory) and equal-energy initial conditions at the onset of slow-roll inflation. We provided analytic and numerical calculations of the intermediate phase after the slow-roll conditions are violated for heavy fields, but before preheating commences. We find that the majority of the energy at the onset of preheating is carried by the axions with light masses, because $\sim$90% of the energy is carried by only $\sim$10% of the fields. Thus, only these light fields need to be taken into account during preheating. To study preheating, we coupled a single massless bosonic matter field χ to the axions φ_i, assuming the same coupling constant g^2 between χ and φ_i. Within this setup, we solved for the evolution of the matter field numerically, including the expansion of the Universe, and found power-law–like behavior in short time scales and occasional, not very frequent resonance amplifications in long time scales in the parameter region that would give rise to stochastic resonance in single-field models. In particular, the growth of the matter field is generically not strong enough to resist redshifting due to cosmic expansion. As a result, the old theory of perturbative preheating (see e.g. [25]) applies to this scenario and not parametric resonance models. The outcome is desirable for the model, as there is no danger of producing unwanted relics. The prediction of this model is hence rather different from the accepted view that parametric resonance effects are crucial for preheating [3].

The analysis presented in this paper is dependent upon several assumptions, such as the chosen matter content and coupling constants. In particular, we considered only one matter field coupled to the whole spectrum of axion fields with the same coupling strength g. Although we believe this choice to be reasonable and the model to be rather generic, dropping some of the assumptions might change the scenario. For instance, it is argued in [33,38] that the oscillations of multiple inflatons (with irrational mass ratios) can enhance drastically the decay rate (Cantor preheating). This argument is based on two pillars: first, theorems in spectral theory indicate that stability bands vanish [33,34,38] in the case of more fields whose masses are not related by rational numbers. Second, numerical evidence in two field models indicates a slight enhancement of particle production for well-chosen parameters [38]. In the latter study of Cantor preheating, dephasing of fields is unimportant since only two fields are considered. Nevertheless, an enhancement effect like in Cantor preheating cannot be excluded in $\mathcal{N}$-flation, especially if only a few axions couple to a given matter field.

Besides Cantor preheating, we would like to comment on yet another effect. It has been shown in [54,55] that noise on top of an oscillating driving force can also enhance resonant particle production.[3] This phenomenon could also occur in multifield inflation, if preheating is dominated by one or two fields: the oscillations of the many other fields would then act similar to noise, potentially enhancing preheating.

Further, we have ignored backreaction and rescattering during preheating, since modifications due to these two effects should be minor. Explosive χ-particle production due to parametric resonance is irrelevant in $\mathcal{N}$-flation, as argued above, so that $\langle\chi^2\rangle$ remains small; in addition, their inclusion would only diminish resonance effects further.

ACKNOWLEDGMENTS

We thank Thorsten Battefeld and Richard Easther for early discussions motivating this work, as well as helpful conversations with Shinta Kasuya. We also thank Kari Enqvist and Dmitry Podolsky for helpful comments. D. B. is supported by the EU FP6 Marie Curie Research and Training Network "UniverseNet" (MRTN-CT-2006-035863). S. K. is supported by the Academy of Finland Finnish-Japanese Core Programme Grant No. 112420. Some of the numerical calculations were carried out using computing facilities at the Yukawa Institute, Kyoto University.

APPENDIX: FURTHER ANALYTIC ESTIMATES

In Sec. III A we developed a semianalytic solution (I) which underestimates the numerical values of the potential energy W (see Table I). Here we present a second analytic approximation, which we call solution (II), that gives an upper bound for W after the slow-roll condition for the heaviest field is violated, to check the numerical solution in Table I. In addition, both analytic solutions can be used for arbitrarily large numbers of fields that would not be tractable via a brute force numerical integration.

The basic idea consists of holding fixed heavy fields as soon as the corresponding η becomes of order 1: first, we take the continuum limit so that we can make use of the Marčenko-Pastur law for the continuous mass variable $1 \leq x \leq \xi$. Second, we partition this interval into $\mathcal{M}$ bins according to a simple rule and denote the upper boundaries of bins with X_A, $A = 1, \ldots, \mathcal{M}$, so that $X_{\mathcal{M}} = \xi$. Third, whenever η_A (corresponding to some X_A) becomes of order 1, we hold fixed all fields with masses in the Ath bin. Naturally, one recovers the full microscopic model if

[3]However, see [56].

TABLE III. Semianalytic solution II for $\mathcal{N} = 200, 400, 1500$, to be compared with the slow-roll result I from Table I. Here, R is the ratio between the potential energy of the heavy (held-fixed) fields to that of the light (dynamical) ones. We use a mass splitting into $\mathcal{M} = 50$ bins. X_1 is chosen such that $\sigma_{II}(Y_{\mathcal{M}}) \approx \sigma_I(y_{\rm end})$. The approximation (II) approaches the slow-roll result for increasing $\mathcal{N}$. The numerical results in Table I lie nestled between the two approximations.

$\mathcal{N}$	X_1	$\sigma_{II}(Y_{\mathcal{M}})$	$W_{II}(Y_{\mathcal{M}})$	$\frac{W_{II}(Y_{\mathcal{M}})}{W_I(y_{\rm end})}$	$\frac{N_{II}(Y_{\mathcal{M}})}{N_I(y_{\rm end})}$	R
200	2.90	5.40	2.91	1.47	1.07	0.97
400	2.15	8.32	2.15	1.24	1.01	0.74
1500	1.75	17.57	1.75	1.17	1.00	0.53

one takes $\mathcal{M} = \mathcal{N}$ and uses the Marčenko-Pastur law as a rule for choosing the bins so that $X_A = \tilde{m}_A^2/m_0^2$.

Taking $\mathcal{M} < \mathcal{N}$ leads to a coarse-grained model which is more tractable, but one pays the price of having a larger W. This approximation is justified as long as the energy left in the heavy fields is small compared to the energy in the light fields; $\mathcal{M} \sim 50$ suffices for the range of y-values that we are interested in.[4]

We now proceed to compute W_{II}, σ_{II} and N_{II} as outlined above. We assume first a partition $\{X_1, \ldots, X_{\mathcal{M}}\}$ of the interval $1 \leq x \leq \xi$ and denote with Y_A the values of y where $\eta_{(\mathcal{M}-A+1)} = 1$ (note that $Y_A < Y_B$ if $A > B$). If we further denote the energy W_{II} that is valid in the range $Y_A < y < Y_{A-1}$ with W_A, we can calculate the corresponding Y_A as the solution to

$$W_A(Y_A) = m_0^2 X_{\mathcal{M}-A+1}, \tag{A1}$$

starting with $W_1 \equiv W_I$. Note that $Y_1 = y_{\mathcal{N}}$ from (31), as it should. We can then compute W_A for $A \geq 2$ to

$$W_A(y) = \frac{\mathcal{N}}{2} m_0^2 \varphi_0^{*2} \left(\langle y^x \rangle|_1^{X_{\mathcal{M}-A+1}} + \sum_{n=1}^{A-1} \langle Y_n^x \rangle|_{X_{\mathcal{M}-n}}^{X_{\mathcal{M}-n+1}} \right). \tag{A2}$$

Similarly, if we denote with σ_A the effective field which is valid in the range $Y_A < y < Y_{A-1}$ (so that $\sigma_1 = \sigma_I$), we arrive at

$$\sigma_A(y) = \sigma_{A-1}(Y_{A-1}) + \frac{\sqrt{\mathcal{N}}}{2} \varphi_0^* \int_y^{Y_{A-1}} \frac{1}{s} \sqrt{\langle x s^x \rangle|_1^{X_{M-A+1}}}\, ds, \tag{A3}$$

and finally the number of e-folds becomes (with $Y_0 = 1$)

$$N_A(y) = N_{A-1}(Y_{A-1}) + \int_y^{Y_{A-1}} \frac{W_A(s)}{2m_0^2 s}\, ds. \tag{A4}$$

In an appropriate large $\mathcal{M}$-limit the above approximation becomes independent of the partition, which is of course our aim. We would like to use W_{II} up to when W_I is no longer a viable lower bound for the true energy W, that is, until $\sigma \approx \sigma_I(y_{\rm end})$. This is possible by tuning X_1 such that $\sigma_{II}(Y_{\mathcal{M}}) \approx \sigma_I(y_{\rm end})$.[5]

That way, the energy ratio of heavy to light fields becomes

$$R \equiv \frac{W_{\rm heavy}}{W_{\rm light}} = \frac{\frac{2}{\mathcal{N} m_0^2} W_{II}(Y_{\mathcal{M}}) - \langle Y_{\mathcal{M}}^x \rangle|_1^{X_1}}{\langle Y_{\mathcal{M}}^x \rangle|_1^{X_1}} \tag{A5}$$

which has to be smaller than 1 (see Table III), so that we can trust our approximation.

We compare (I) and (II) solutions in Table III, where we also vary the number of fields. The solutions approach each other in the large $\mathcal{N}$ limit. Henceforth, the numerical solution is well approximated by either one in the case of $\mathcal{N}$-flation, where we deal with thousands of fields, and consequently, we are justified to use the slow-roll approximation to set the initial stage for preheating.

[4]Note, generically $\sigma_I(y) \neq \sigma_{II}(y)$ because first, a number of fields are artificially held fixed and no longer contribute to the path length σ, and second, the total potential energy is bigger so that light fields evolve slightly slower. Only small corrections result, since fixed fields are already near the minimum of their potential, not contributing much to σ anyhow. Moreover, we demand $R < 1$. Consequently, we have $y_{II} \sim y_I$ and $\sigma_{II} \sim \sigma_I$.

[5]We choose X_1 as large as possible so that $R < 1$, while keeping X_1 small enough to ensure that the solution (II) remains applicable up until σ_I leaves slow roll; thus we demand $\sigma_{II}(Y_{\mathcal{M}}) \approx \sigma_I(y_{\rm end})$, leading to $X_1 = 1.75$ for $\mathcal{N} = 1500$. Simultaneously, to distribute the remaining bins, we choose $(\mathcal{M} - 2)/2$ narrow bins from X_1 to $X_{\mathcal{M}/2} \approx 11$ (the MP-distribution peaks in that region), followed by larger bins up until $X_{\mathcal{M}} = \xi \approx 34$. For $\mathcal{N} = 1500$ even $\mathcal{M} \lesssim 50$ yield results insensitive to the chosen partition.

[1] The Planck Collaboration, arXiv:astro-ph/0604069.
[2] D. Wands, Lect. Notes Phys. **738**, 275 (2008).
[3] B. A. Bassett, S. Tsujikawa, and D. Wands, Rev. Mod. Phys. **78**, 537 (2006).
[4] S. Dimopoulos, S. Kachru, J. McGreevy, and J. G. Wacker, arXiv:hep-th/0507205.
[5] K. Becker, M. Becker, and A. Krause, Nucl. Phys. **B715**, 349 (2005).
[6] M. Majumdar and A.-C. Davis, Phys. Rev. D **69**, 103504 (2004).
[7] P. Kanti and K. A. Olive, Phys. Rev. D **60**, 043502 (1999).
[8] P. Kanti and K. A. Olive, Phys. Lett. B **464**, 192 (1999).
[9] A. R. Liddle, A. Mazumdar, and F. E. Schunck, Phys. Rev. D **58**, 061301 (1998).
[10] E. J. Copeland, A. Mazumdar, and N. J. Nunes, Phys. Rev. D **60**, 083506 (1999).
[11] H. Singh, Mod. Phys. Lett. A **22**, 2737 (2007).
[12] N. Kaloper and A. R. Liddle, Phys. Rev. D **61**, 123513 (2000).
[13] R. Easther and L. McAllister, J. Cosmol. Astropart. Phys. 05 (2006) 018.
[14] S. A. Kim and A. R. Liddle, Phys. Rev. D **74**, 023513 (2006).
[15] S. A. Kim and A. R. Liddle, Phys. Rev. D **74**, 063522 (2006).
[16] Y.-S. Piao, Phys. Rev. D **74**, 047302 (2006).
[17] T. W. Grimm, arXiv:0710.3883.
[18] L. Alabidi and D. H. Lyth, J. Cosmol. Astropart. Phys. 05 (2006) 016.
[19] D. Battefeld and T. Battefeld, J. Cosmol. Astropart. Phys. 05 (2007) 012.
[20] D. H. Lyth and A. Riotto, Phys. Rep. **314**, 1 (1999).
[21] E. Komatsu *et al.* (WMAP Collaboration), arXiv:0803.0547.
[22] A. D. Dolgov and A. D. Linde, Phys. Lett. **116B**, 329 (1982).
[23] A. D. Dolgov and D. P. Kirilova, Sov. J. Nucl. Phys. **51**, 172 (1990).
[24] J. H. Traschen and R. H. Brandenberger, Phys. Rev. D **42**, 2491 (1990).
[25] L. Kofman, A. D. Linde, and A. A. Starobinsky, Phys. Rev. D **56**, 3258 (1997).
[26] Y. Shtanov, J. H. Traschen, and R. H. Brandenberger, Phys. Rev. D **51**, 5438 (1995).
[27] S. Y. Khlebnikov and I. I. Tkachev, Phys. Rev. Lett. **77**, 219 (1996).
[28] S. Y. Khlebnikov and I. I. Tkachev, Phys. Lett. B **390**, 80 (1997).
[29] S. Y. Khlebnikov and I. I. Tkachev, Phys. Rev. Lett. **79**, 1607 (1997).
[30] T. Prokopec and T. G. Roos, Phys. Rev. D **55**, 3768 (1997).
[31] D. I. Podolsky, G. N. Felder, L. Kofman, and M. Peloso, Phys. Rev. D **73**, 023501 (2006).
[32] J. F. Dufaux, G. N. Felder, L. Kofman, M. Peloso, and D. Podolsky, J. Cosmol. Astropart. Phys. 07 (2006) 006.
[33] B. A. Bassett, Phys. Rev. D **58**, 021303 (1998).
[34] J. Moser, *Integrable Hamiltonian Systems and Spectral Theory* (Lezioni Fermiane, Accad. Naz. Lincei and Scuola Norm. Sup., Pisa, 1981).
[35] I. I. Gihman and A. V. Skorohod, *The Theory of Stochastic Processes I, II, II* (Springer, New York, 1979).
[36] W. Kirsch, *Lyapunov Exponents, Proceedings*, edited by L. Arnold and V. Wilhstutz (Springer-Verlag, Berlin, 1986).
[37] L. Pastur and A. Figotin, *Spectra of Random and Almost-Periodic Operators* (Springer-Verlag, Berlin, 1991).
[38] B. A. Bassett and F. Tamburini, Phys. Rev. Lett. **81**, 2630 (1998).
[39] I. Zlatev, G. Huey, and P. J. Steinhardt, Phys. Rev. D **57**, 2152 (1998).
[40] D. Green, Phys. Rev. D **76**, 103504 (2007).
[41] A. Krause, arXiv:0708.4414.
[42] D. Podolsky and K. Enqvist, arXiv:0704.0144.
[43] K. A. Malik and D. Wands, Phys. Rev. D **59**, 123501 (1999).
[44] S. Kachru, R. Kallosh, A. Linde, and S. P. Trivedi, Phys. Rev. D **68**, 046005 (2003).
[45] J.-O. Gong, Phys. Rev. D **75**, 043502 (2007).
[46] T. Battefeld and R. Easther, J. Cosmol. Astropart. Phys. 03 (2007) 020.
[47] C. Gordon, D. Wands, B. A. Bassett, and R. Maartens, Phys. Rev. D **63**, 023506 (2000).
[48] M. Sasaki and E. D. Stewart, Prog. Theor. Phys. **95**, 71 (1996).
[49] C. L. Bennett *et al.* (WMAP Collaboration), Astrophys. J. Suppl. Ser. **148**, 1 (2003).
[50] D. N. Spergel *et al.* (WMAP Collaboration), Astrophys. J. Suppl. Ser. **148**, 175 (2003).
[51] H. V. Peiris *et al.* (WMAP Collaboration), Astrophys. J. Suppl. Ser. **148**, 213 (2003).
[52] P. B. Greene, L. Kofman, A. D. Linde, and A. A. Starobinsky, Phys. Rev. D **56**, 6175 (1997).
[53] N. W. McLachlan, *Theory and Application of Mathieu Functions* (Clarendon Press, Oxford, 1951).
[54] V. Zanchin, J. Maia, A. W. Craig, and R. H. Brandenberger, Phys. Rev. D **57**, 4651 (1998).
[55] V. Zanchin, J. Maia, A. W. Craig, and R. H. Brandenberger, Phys. Rev. D **60**, 023505 (1999).
[56] M. Ishihara, Prog. Theor. Phys. **114**, 157 (2005).